Ghahfarokhi, Payam Shams; Kallaste, Ants; Podgornovs, Andrejs; Belahcen, Anouar; Vaimann, Toomas

Development of analytical thermal analysis tool for synchronous reluctance motors

Published in:
IET Electric Power Applications

DOI:
10.1049/iet-epa.2020.0237

Published: 01/10/2020

Document Version
Peer-reviewed accepted author manuscript, also known as Final accepted manuscript or Post-print

Please cite the original version:
Ghahfarokhi, P. S., Kallaste, A., Podgornovs, A., Belahcen, A., & Vaimann, T. (2020). Development of analytical thermal analysis tool for synchronous reluctance motors. *IET Electric Power Applications*, *14*(10), 1828-1836. https://doi.org/10.1049/iet-epa.2020.0237

Development of Analytical Thermal Analysis Tool for Synchronous Reluctance Motors

Payam Shams Ghahfarokhi [1, 2*], Ants Kallaste [2], Andrejs Podgornovs[1], Anouar Belahcen[2, 3], Toomas Vaimann[2]

[1] Institute of Electrical Machinery and Equipment, Riga Technical University, Kaļķu iela 1, Riga, Latvia
[2] Electrical Power Engineering and Mechatronics, Tallinn University of Technology, Ehitajate tee 5, Tallinn, Estonia
[3] Electrical Engineering and Automation, Aalto University, Espoo, Finland
*payam.shams@taltech.ee

Abstract: This paper presents the principles of analytical lumped parameter (LP) model for a Synchronous reluctance motor (SynRM) for traction application purposes. Particular focus is put on the calculation of the heat transfer from the machine's housing during the active and passive cooling. For this purpose, the area-based composite correlations method is proposed. The approach is attractive due to its simplicity and the fact that it closely models the temperature of the machine's housing. Finally, the proposed thermal model is evaluated experimentally on a totally enclosed fan cooled (TEFC) SynRM, and good correspondence between the analytical and experimental results is obtained.

1. Introduction

According to the European Union target to mandatory minimizing the CO2 emissions, there is a massive interest in the research and development of the electrical motors for traction applications. The electrical motors using for electric vehicles have high power density and compact structure [1], [2]. Accordingly, the accurate thermal analysis of the electrical machine is one of the most critical sections in the design process of the electrical motors, which is playing a vital role in the performance, power density, and energy efficiency of the electrical motors. One of the types of electrical motors attracting the attention for traction application purposes is synchronous reluctance motor (SynRM) with a transverse-laminated rotor [3]. Several research papers considered this type of motor as an alternative option for traction application purposes such as railway [4]-[5]. These types of motors have a low expense, robustness, simple structure, and manufacturing process [3], [6]-[7].

Analytical and numerical models are major approaches in the thermal evaluation of an electrical machine [8]-[9]. In the analytical approach, the lumped parameter (LP) model is developed to capture the temperature of critical parameters of the machine. This approach is a prompt computation technique with reasonable precision [10].

The finite element (FE) model and computational fluid dynamic (CFD) are the conventional numerical methods in the temperature calculation [11]. FE model is a suitable approach to model heat transfer in solid materials [12]. However, CFD is an accurate approach to assess the flow rate, coolant distribution, and convection heat transfer [12]. The drawbacks of numerical methods are high setup and computation time [12]. Furthermore, for thermal modeling of the entire electrical machine, these two methods should be conjugated [13].

Consequently, LPTN is the main method for fast thermal analysis. Many studies apply the analytical LPTN method for thermal calculation[14]-[15]. Mellor in [16] presented one of the earlier studies in this field, where he developed an LPTN for TEFC induction machine. He modeled heat transfer in the machine in radial and axial orientations. Accordingly, his model consisted of several convection paths, which enhanced the complexity of the thermal network and the computing process.

Furthermore, he determined the heat transfer coefficient from the housing to the ambient directly from the experiment. In the following, Boglietti in [17] demonstrated his LP thermal model for variable speed self-cooled industrial induction motors. He implemented several hypotheses to decrease the complexity of the thermal model as well as calculation time by saving the calculation precision. However, in his model, he neglected the heat transfer by radiation mechanism.

Moreover, he assessed several critical components, e.g., the thermal conductivity of slot, the interface gap resistance, and heat transfer resistance from the housing to the ambient by setting up a proper thermal test. In addition, he did not segregate the active and end winding parts. Finally, he applied the simplifying assumption to calculate the forced convection coefficient from the machine surfaces by neglecting fins structures of housing and assuming the machine housing as a smooth cylinder.

One of the first studies on the thermal designs of permanent magnet (PM) machines was presented by Lindstrom in 1999 [18]. He developed the analytical thermal model for the surface-mounted PM machine to estimate the thermal behavior of the machine during the steady-state and transient modes. His work was not contained the convection and radiation phenomena from the machine housing to the coolant and directly connected the thermal model of the

machine to the coolant. Furthermore, he evaluated the equivalent length of the interface gap according to the material type of the machine housing and power rate of the machine. In [19], El-Refaie developed a thermal model for the interior permanent magnet (IPM) synchronous machine based on the proposed thermal model of Lindstrom and only altering the rotor LP circuit and suffer the same drawbacks of Lindstrom model.

This paper presents a detailed analytical thermal analysis of a SynRM. The research aims are to increase knowledge in the thermal calculation of the electrical machine and develop the analytical thermal calculation tool for SynRMs. The paper concentrates on the mentioned challenges in ongoing product development. The main objective is to develop modified analytical LPTN that is used in the thermal calculation of electrical machines, and then implement them for a SynRM machine. The advantages of the developed LPTN are reducing the complexity of the analytical model of the machine, saving the accuracy to estimate the temperature of the critical components of the machine, and decreasing the calculation time. To clarify the research topic, it mainly focuses on the thermal aspect, including passive and active cooling. The passive cooling refers to the effectiveness of heat distribution within a machine, which is affected by material thermal properties, geometrical design, and interfacial thermal resistances between machine components. For example, the passive thermal design of a stator slot strongly influences the temperature gradient of the coil. Active cooling refers to the effects of heat extraction from a machine to the coolant, ultimately based on the convection phenomenon.

For the research purposes, the thermal models described in this study are applied to SynRM with a four poles 10 kW, 400 V, 50 Hz, and 'F' insulation class. Fig. 1 illustrates the structure and topology of the machine. This machine is a totally enclosed fan cooled machine, and it uses the air forced cooling method. Accordingly, the fin channel design is essential in the outer peripheral of the housing. An analytical model of the machine is developed, and the calculation of its components is explained. Finally, to validate the analytical model, an experimental setup and measurements are carried out. The test outcomes are used to validate the analytical data.

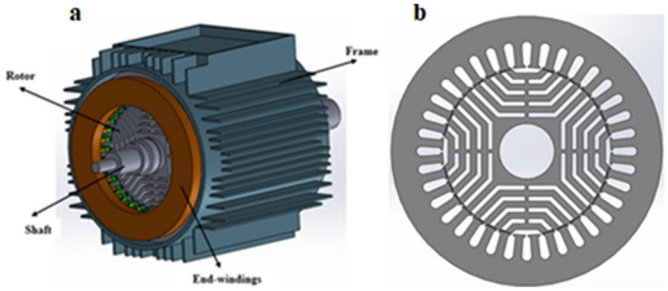

Fig. 1. *CAD drawing of the SynRM*

2. Lumped Parameter Thermal Modeling

Due to the risk of high temperature inside the slot and damaging the slot insulation, which reduces the lifetime of the insulation materials as well as the machine life, precise prediction of the temperature distribution in the machine is necessary.

An electrical machine consists of complex geometries; to model the temperature distribution inside the machine with high accuracy and resolution, a large thermal network to involve all thermal paths is needed. However, the large thermal network with a high number of nodes enhances the computation time and the complexity of the model. Furthermore, some variable parameters such as convection coefficients require a complicated calculation process due to complex geometries and the unknown flow condition. As a result, during the design process of an electrical machine, a fast and compact model, which predicts the temperature of the critical components of the electrical machine, is needed. Consequently, it is necessary to implement the geometrical symmetries and some hypotheses such as a uniform distribution of losses inside the machine; the focus of the heat transfer in the axial direction is on the shaft and the stator windings, uniform distribution of the temperature in the machine housing. The effect of these symmetries and hypotheses on the model is in reducing the number of thermal paths and nodes, calculating the conduction resistances to model the heat paths in the machine lamination easily by hollow cylinder correlation, and reducing the order and complexity of the LPTN.

Fig. 2 shows the steady-state LP model for the SynRM under discussion. The model consists of six nodes that feature all the critical thermal components and temperature rises. Since the significant portion of the heat is generated inside the slots, and the end-windings are usually the hottest parts of the machine, the stator windings are the key component in the SynRM where the temperatures are particular interest during the design process. Therefore, two separate nodes are assigned to estimate the temperature of the stator coil embedded inside the slots (node 4), and the end windings (node 5). Furthermore, Network nodes are also assigned to estimate the temperature of machine housing (node 1), stator yoke (node 2), stator teeth (node 3), and the rotor (node 6) to complete the model.

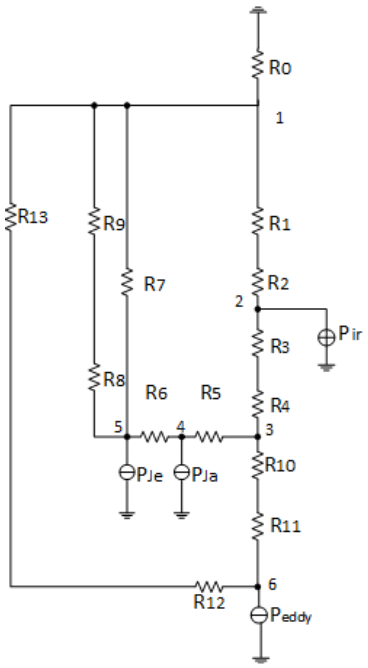

Fig. 2. *The LP thermal model.*

Moreover, among the different nodes, there are thermal resistances to model the heat transfer paths as well as heat sources to model the losses in the machine. In total, there are 14 thermal resistances and four heat sources. Table 1 gives the definitions of these resistances and sources.

Table 1 Description of thermal resistances

Component	Description
R_0	thermal resistance from the frame to ambient
R_1	Conduction resistance of the Interface gap between the frame and stator laminations
R_2	Conduction resistance of the upper half side of the stator core back
R_3	Conduction resistance of the lower half side of the stator core back
R_4	Conduction resistance of the stator teeth
R_5	Conduction resistance between the stator slots and the stator teeth
R_6	Conduction resistance between the coil side and the end-windings
R_7	Conduction resistance between the stator winding and the housing
R_8	Convection resistance between the stator end-winding and the end region
R_9	Convection resistance between the end region and the end cap
R_{10}	Convection resistance of the air gap
R_{11}	Conduction resistance of the upper half side of the rotor
R_{12}	Conduction resistance of the lower half part of the rotor
R_{13}	Axial conduction of the shaft
P_{ir}	Iron losses in the stator
P_{Ja}	Active copper losses
P_{Je}	End –winding copper losses
P_{eddy}	Iron losses in the rotor

3. Computation and identification of the LPTN parameters

In this section, the computing methods of the thermal network resistances by analytical and empirical correlations are described. For these purposes, some geometry simplifications are implemented, which are discussed in the following. First, this section focuses on the calculation of the conductive resistances in the stator and the rotor. Finally, it considers the heat transfer paths by convection and radiation phenomena.

Detailed information on the geometrical data of the motor is given in Table 2, and the material properties of the machine are presented in Table 3.

Table 2 Geometrical data

Name	Symbol	Unit	Value
Stator core length	L_s	mm	156
Stator inner diameter	D_{is}	mm	136
Stator outer diameter	D_{os}	mm	219
Number of slots	N_s	-	36
Air-gap height	l_g	mm	0.4
Rotor inner diameter	D_{ir}	mm	45
Rotor outer diameter	D_{or}	mm	135.2
Slot height	H_{slot}	mm	21
Slot filling factor	k_f	-	0.6
Slot area	S_{lots}	mm^2	130.1

Table 3 Material properties

Machine part	Material	Thermal conductivity symbols	Thermal conductivity (W/m-K)
Frame	Aluminum	k_{al}	230
Laminations	M-350-50A	k_{ir}	28
Winding	Copper	k_{cu}	387
Impregnation	Resin	k_{res}	0.2
Air gap	Air	k_{air}	0.0257
Shaft	Steel	k_{sh}	41

The conventional form of conduction thermal resistance is defined as [20]:

$$R_{th} = \frac{L}{kA}, \tag{1}$$

where L is the characteristic length (m), k is the thermal conductivity of the material (W/m-K), and A is the cross-section area (m^2).

Moreover, the general equation for the calculation of the conduction resistance from the radial direction of the hollow cylinder and the cylindrical section are defined respectively as [19], [21]:

$$R_{th} = \frac{\ln(\frac{r_{out}}{r_{in}})}{2\pi kL}, \tag{2}$$

$$R_{th} = \frac{\ln(\frac{r_{out}}{r_{in}})}{kL\varphi}, \tag{3}$$

where r_{out} is the outer radius (m), r_{in} is the inner radius (m), and φ is the angular span (rad).

By using equations (1), (2), and (3) and relevant geometric and thermal data represented in Tables 1 and 2, the values of conductive resistances in the thermal network in Fig. 2 are calculated and summarized hereafter.

Interface gap conduction resistance (R_1):

The interface gap occurs during the assembling process of packing the stator to the housing, and it is evaluated as [17]:

$$R_1 = \frac{l_{ig}}{k_{air}\pi D_{os}L_s}, \tag{4}$$

where l_{ig} is the interface gap between the frame and stator laminations (m), which is selected according to [22].

Stator yoke conduction resistances (R_2 and R_3):

According to Fig. 3, the stator yoke is divided into two sections, and the value of the radial conduction resistance of each part is evaluated by using (2) as follows [17]:

$$R_2 = \frac{\ln(\frac{r_{os}}{r_m})}{2\pi k_{ir} L_s}, \quad (5)$$

$$R_3 = \frac{\ln(\frac{r_m}{r_{iy}})}{2\pi k_{ir} L_s}, \quad (6)$$

where r_m is the mean value of the stator yoke radius (m), r_{oy} is the outer radius of the stator, and r_{iy} is the inner radius of the stator yoke (m).

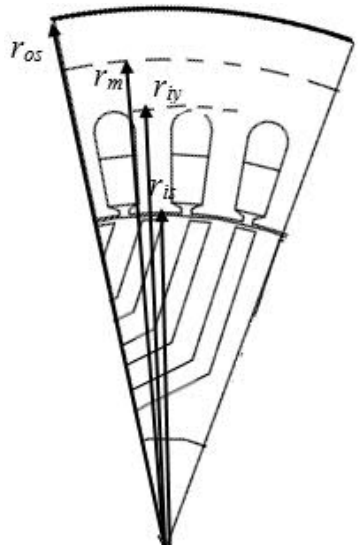

***Fig. 3**. The stator core radial dimensions.*

Stator teeth conduction resistance (R_4):

To evaluate the equivalent thermal resistance of the stator teeth, the geometry of this motor portion is assumed as a cylinder. To reduce the slots section and assess the value of the thermal resistance of the teeth, one reduction factor (p_{th}), which equals the percentage of teeth volume iron to the total volume of the teeth and slots is applied to the formula [17].

$$R_4 = \frac{ln(\frac{r_{iy}}{r_{is}})}{2\pi k_{ir} L_s p_{th}}, \quad (7)$$

where r_{is} is the inner stator radius (m).

Conduction thermal resistance from stator windings (R_5 and R_6):

The stator winding is an essential section of thermal modeling. A significant part of the heat is produced there. This section includes of several materials with high thermal sensitivity, which increases the importance of accurate modeling of this part.

Heat fluxes in the slot are released in axial, radial, and circumferential directions. The axial path presents the heat flux path from end windings to the slots or vice versa. Radial and circumferential paths represent the heat flow paths to coolant medium by means of the stator core. Consequently, the stator winding is divided into resistances R_5 and R_6 to model the circumferential and the axial heat transfer, respectively.

R_5 presents the conduction paths for the heat flow in the radial and circumferential part of the stator slot and is evaluated as in [17]:

$$R_5 = \frac{t_{eq}}{k_{ins} A_{slot}}, \quad (8)$$

where t_{eq} *is* the equivalent thickness of impregnation insulation materials in the stator slot (m), k_{ins} is the equivalent thermal conductivity of insulation materials in the stator slot (W/m-K), and A_{slot} is the interior slot surface (m^2).

The equivalent thermal conductivity of the slot can be evaluated by three methods: layer winding, cuboidal and equivalent insulation. In this research paper, the equivalent insulation method is applied to find the equivalent conductivity of the slot. This method is a fast calculation method and can be easily used by knowing the slot-filling factor. Based on this method, copper has high thermal conductivity and low conduction thermal resistance. Consequently, the copper thermal resistance can be neglected in the analytical model of the stator winding in the circumferential and radial direction. Figure 4 shows a simplified assumption to model the equivalent insulation method in the active part of the slot. As a result, the equivalent thermal conductivity of the insulation k_{ins} is assessed by a liner empirical correlation as in [22]:

$$k_{ins} = 0.1076 k_f + 0.029967 . \quad (9)$$

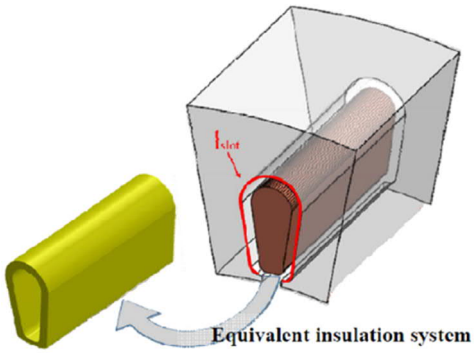

***Fig. 4.** Equivalent insulation method in the stator slot* [23].

R_6 presents the thermal conduction path from the end winding to the slot, and it is computed as in [18]:

$$R_6 = \frac{l_{av}}{6\, N_s k_{cu} S_{cu}} . \quad (10)$$

where l_{av} is the average conductor length of half a turn (m), N_s is the number of the stator slots, k_{cu} is the thermal conductivity of the copper (W/m-K), S_{cu} is the total copper conductor cross-section area (m^2)

Conduction resistance between the end windings and the motor housing (R_7):

The distance between the outer surface of the end winding and the internal part of the machine housing is low [20]; accordingly, the airspeed in this region is very low, and the heat exchange from the end winding to the internal part of the housing is assumed as conduction and is calculated as:

$$R_7 = \frac{ln\left(\frac{r_{os}}{r_{os}-\gamma H_y}\right)}{2\pi k_{air}(L_{ec}-L_s)}, \quad (11)$$

where H_y is the stator yoke height (m), γ is the reduction coefficient to implement the distance between the outer surface of the end winding, and the internal part of the housing and L_{ec} is the motor housing length (m).

The value of γ for ordinary induction machines with single layer windings is defined in the range of 0.4 to 0.7 [17]. However, this value for the machine by the double layer windings decreases to the range of 0.25 to 0.4 [3].

Conduction resistances of the rotor (R_{11} and R_{12}):

Fig. 5 illustrates the cross section of a one eighth of the rotor. The rotor structure is formed from the steel laminations, as the magnetic flux paths and air gaps in the laminations as magnetic flux barriers. As the heat inside the flux barriers is transferred by the natural convection and according to the high thermal conductivity of the steel laminations, consequently, the heat transfer by the natural cooling from barriers is eliminated and assumed whole of the heat is transferred by the conduction mechanism through the steel laminations.

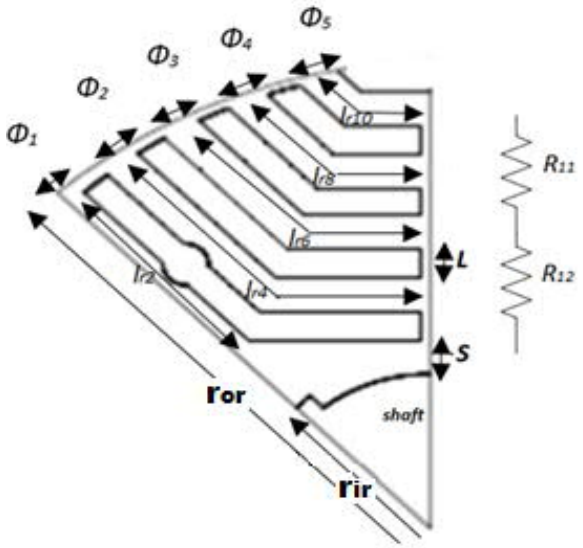

Fig. 5*. The half of pole of the rotor.*

Fig. 6 illustrates the LP circuit of the rotor by implementing the above simplifying hypothesis. According to Fig. 5, the total value of the rotor resistance equals *Rr*, which consists of the series-parallel combinations of thermal resistances. To implement the rotor losses to the LPTN, *Rr* is divided into two equal resistances R_{11} and R_{12} illustrated in Fig.5 and the LPTN of the SynRM.

The value of the thermal resistances presented in Fig. 6 is calculated by (1) and (3). The values of R_{1r} and R_{11r} to R_{15r} are calculated by (3), and the rest are evaluated by (1). Tables 4 and 5 provide a better overview of the computation of the conduction resistances.

Finally, the value of *Rr* is calculated by the series-parallel resistances law in the electrical circuit. Further, R_{11} and R_{12} are defined as:

$$R_{11} = R_{12} = \frac{Rr}{2}. \quad (12)$$

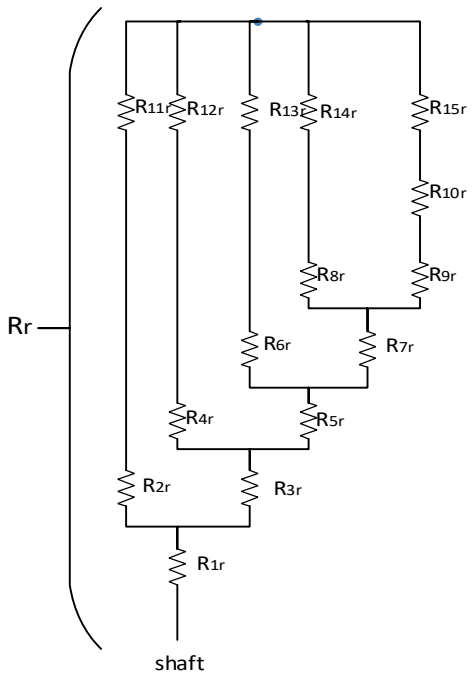

Fig. 6. *Equivalent thermal circuit of the rotor.*

Table 4 Calculation of the radial thermal resistance by (3)

Resistance	r_{out}	r_{in}	k	φ
R_{1r}	$r_{ir}+s$	r_{ir}	k_{ir}	$\pi/4$
R_{11r}	r_{or}	r_{or}-1	k_{ir}	Φ_1
R_{12r}	r_{or}	r_{or}-1	k_{ir}	Φ_2
R_{13r}	r_{or}	r_{or}-1	k_{ir}	Φ_3
R_{14r}	r_{or}	r_{or}-1	k_{ir}	Φ_4
R_{15r}	r_{or}	r_{or}-1	k_{ir}	Φ_5

Table 5 Calculation of the thermal resistances by (1)

Resistance	L	k	A
R_{2r}	l_{r2}	k_{ir}	A_{2r}
R_{3r}	L	k_{ir}	A_{3r}
R_{4r}	l_{r4}	k_{ir}	A_{4r}
R_{5r}	L	k_{ir}	A_{5r}
R_{6r}	l_{r6}	k_{ir}	A_{6r}
R_{7r}	L	k_{ir}	A_{7r}
R_{8r}	l_{r8}	k_{ir}	A_{8r}
R_{9r}	L	k_{ir}	A_{9r}
R_{10r}	l_{r10}	k_{ir}	A_{10r}

Axial conduction thermal resistance of the shaft (R_{13}):

According to the hypothesis, the axial heat transfer in the rotor is considered in the shaft, and by using the simplifying assumption that the temperature distribution along the shaft is uniform, R_{13} is calculated as:

$$R_{13} = \frac{1}{4}\left(\frac{0.5L_s}{k_{ir}\pi r_{ir}^2}\right) + \frac{1}{2}\left(\frac{0.5(L_{shaft}-L_s)}{k_{ir}\pi r_{ir}^2}\right). \quad (13)$$

where L_{shaft} is the length of the shaft (m), and r_{ir} is the inner radius of the rotor (m).

R_{13} is made of two contributions. The first one represents the shaft part below the rotor core (radial heat from the rotor to the shaft), and the second one is model the axial thermal resistance due to the shaft part external to the rotor core length.

Thermal resistance from the machine housing to the ambient (R_0):

A significant part of the heat in the TEFC machine is dissipated from the machine housing to the surroundings by the combination of radiation and convection phenomena. The radiation occurs in parallel with the convection, and it is difficult to segregate these two phenomena from each other. Accordingly, it is conventional to add these coefficients together and define the heat transfer coefficient in the analysis. Therefore, the heat transfer resistance from the motor 's housing to the surroundings is defined as:

$$R_0 = \frac{1}{h_0 A_T}, \tag{14}$$

where A_T is the machine-housing area (m^2), and h_0 is the heat transfer coefficient from the housing to the ambient (W/ m^2-K).

Accordingly, the critical parameter in the evaluation of this resistance is the heat transfer coefficient (h_0). The heat transfer coefficient (h_0) consists of the effect of the radiation and the convection phenomena and is defined as:

$$h_0 = h_r + h_c. \tag{15}$$

where h_r and h_c are the radiation and convection coefficients (W/m^2-K), respectively.

Consequently, the accurate prediction of these coefficients leads to the higher accuracy of the analytical thermal model.

Radiation is the latest heat transfer phenomenon in the thermal analysis of the electrical machine that has attracted the attention of the experts. The radiation coefficient h_r is calculated as [24]-[25]:

$$h_r = \varepsilon\sigma F(T_1 + T_2)(T_1^2 + T_2^2). \tag{16}$$

where ε is the relative emissivity, σ is the Stefan-Boltzmann constant equals 5.67×10^{-8} (W/m^2-K^4), F is the view factor, T_1 and T_2 are the temperatures of radiating and absorbing surfaces (K) respectively.

Moreover, the convection coefficient (h_c) is often determined by empirical correlations. These correlations have been developed by dimensionless numbers, e.g., Rayleigh (Ra), Grashof (Gr), Prandtl (Pr), and Reynolds (Re) numbers [12].

Natural Cooling:

In the enclosed fan-cooled machine working at low speed or close to the stall, the natural convection heat transfer is dominating the cooling phenomenon [10]. In this manner, generally, the thermal resistance from the housing of the machine to the ambient is the largest thermal resistance from the stator winding to the ambient [10]. Besides, the frame structure of this machine is designed for the forced cooling, and these semi-open fin channels cannot provide a good air path into the depth of the channels during natural cooling [10].

Determining h_0 is a challenging task, especially for TEFC machines, which consist of complex shapes of the machine housing. There is no single empirical correlation to calculate the natural convection coefficient. The area-based composite correlations method is used to overcome the calculating the natural convection coefficient from the complex shape of the TEFC housing [10], [22]. In this method, the machine's housing is divided into several basic shapes with known empirical correlation to calculate the convection coefficient. For the machine under study, the housing is divided into several different basic shapes as the cylinder shape (to model the fin channel base), horizontal U-shape channel (for fins on the top and underside of the housing) and a horizontal flat plate with a hot plate on top or bottom(for fins mounted on the side of the housing), and the vertical flat plate (to model the end cap of the housing).

Most of the studies related to the thermal calculation of electrical machines have neglected the radiation phenomenon according to the statement that the temperature of the stator housing of the motor is not high enough [10], [26]. However, this statement can be correct in the electrical machines such as TEFC machine cooling by the fan at the high motor speed [26]. Nevertheless, in the electrical machine with natural cooling or with very low motor speeds, the above statement is incorrect, and between 20 to 40% of the total heat is extracted by the radiation phenomenon [27], [28].

The radiation resistance can be calculated by (16). However, the radiation calculation of the fins housing of the electrical machine is more complicated than the smooth electrical machine housings. In particular, the calculation of the view factor is a challenging part of the calculation of the radiation coefficient (h_r) [10]. A simplifying assumption is used to reduce the complexity of the radiation calculation. Accordingly, the whole surface with a clear view of the ambient such as fin base, end caps, and fin tips has a view factor equal to one, and the rest with no clear view of the ambient such as fin sides have the view factor equal to zero [29]. Therefore, the heat is extracted to the ambient by radiation only from the fin base, fin tips, and end caps.

Table 6 Segregation of the housing for natural convection

Component	Convection Correlation	Emissivity	View Factor
Fin base	Horizontal cylinder	0.8	1
Fins on top of the housing	Horizontal fin channel	0.8	0
Fins on undersides of the housing	Horizontal fin channel	0.8	0
Fins on the sides of the housing	Horizontal flat plate (upper face and lower face)	0.8	0
Fin tips	Horizontal and vertical flat plate	0.8	1
End caps	Vertical flat plate	0.8	1

Table 6 shows the segregation of the machine housing under study according to the area-based composite correlations method. Accordingly, the natural convection coefficient from each section is calculated by the relevant empirical correlation for convection. These correlations were provided in our previous research papers [30], [31], and they are not repeating it here again. The simplification assumption calculates the radiation coefficient.

Finally, the heat transfer coefficient (h_0) is calculated according to the average area occupied by each shape as [32]:

$$h_0 = \frac{\sum h_i A_i}{A_T}, \quad (17)$$

where h_i is the heat transfer coefficient from shape i (W/ m^2-K), A_i is the area occupied by shape i (m^2), and A_T is the total housing surface of the machine housing (m^2).

Forced Cooling:

The forced convection coefficient can be determined in several ways, e.g., CFD, analytical flow analysis, and empirical correlation [10]. Determining the convection coefficient by the CFD and analytical flow analysis is a complex process with sophisticated calculation; as a result, the convection coefficient during the forced cooling is determined by an empirical correlation. The common correlation to calculate the convection coefficient from semi-open fin channel is presented by Heiles and is defined as [32]:

$$h = \frac{\rho\, c_p D_h\, v}{4L_f}\,(1 - e^{-m}), \quad (18)$$

$$m = 0.1448\,\frac{L_f^{0.946}}{D_h^{1.16}}\left(\frac{k}{\rho\, c_p v}\right)^{0.214}, \quad (19)$$

where D_h is the hydraulic diameter (m), c_p is fluid specific heat capacity (kJ/kg-°C), and k is fluid thermal conductivity (W/m-K), ρ is fluid density (kg/m^3), v is the airspeed (m/s), and L_f is the axial length of the fin channel (m). Finally, the value of the convection coefficient calculated from (18) is multiplied to a correction factor between 1.7 to 1.9 [32].

According to (18), the only unknown parameter with the highest effect on the calculation of the forced convection coefficient is the airflow speed along the semi-open fin channels. To use the empirical correlation, an accurate estimation of the rate of the cooling airflow in each fin is necessary. Accordingly, the amount of the speed of the cooling air is measured by a digital hot wire anemometer.

The housing of the machine is segregated into three parts: rear section near the fan, active section, and front section to calculate the forced convection coefficient from the housing surface of the machine by the empirical correlations and applying the leakage effect on the air-cooling speed during the computation process. Then, the value of the forced convection coefficient is calculated based on the appropriate empirical correlation. Furthermore, the amount of radiation is calculated by the simplifying method discussed previously.

Table 7 shows the segmentation of the machine housing and related empirical correlation for calculating the value of the forced convection coefficient and the radiation phenomenon.

The blockage factor is defined to apply the effect of fin blockage in the calculation of the forced convection coefficient, as [22]:

$$\frac{N_{total} - N_{block}}{N_{total}}, \quad (22)$$

where N_{total} equals to the total number of fins and N_{block} is the number of block fins.

Table7 Segmentation of the housing for the forced convection

Component	Empirical Correlation	Air velocity (p.u)	Emissivity	View Factor
End cap (rear)	Flat plate	1	0.8	1
Fins base (rear)	Fin channel	1	0.8	1
Fin side (rear)	Fin channel	1	0.8	0
Fin tips (rear)	Flat plate	1	0.8	1
Fins base (active)	Fin channel	0.8	0.8	1
Fin side (active)	Fin channel	0.8	0.8	0
Fin tips (active)	Flat plate	0.8	0.8	1
Fins base (front)	Fin channel	0.6	0.8	1
Fin side (front)	Fin channel	0.6	0.8	0
Fin tips (front)	Flat plate	0.6	0.8	1
End cap (front)	Flat plate	0.5	0.8	1

Finally, the heat transfer coefficient is determined by (17).

Convection resistance between the stator end windings and the inner air (R_8):

R_8 presents the heat path from the end winding to the inner air by the convection and is calculated as :

$$R_8 = \frac{1}{A_{ew} h_{ew}}, \quad (23)$$

where A_{ew} is the surface of the end winding in contact with the inner air (m^2), and h_{ew} is the convection coefficient between the end windings and the inner air (W/ m^2-K).

$$A_{ew} = (L_{ec} - L_s)2\pi r_{is}, \quad (24)$$

There are several different empirical correlations to calculate the convection coefficient of the end winding to the end region of the machine. According to [33], the best correlation is :

$$h_{ew} = \begin{cases} 15.5 & v = 0 \\ 41.4 + 6.6\,v & v \neq 0 \end{cases}, \quad (25)$$

where v is defined as:

$$v = r_{or}\omega\eta, \quad (26)$$

where r_{or} is the outer radius of the rotor (m), ω is the rotor angular speed (rad/s), and η is the fan efficiency and in most the cases, equals 0.5.

Convection resistance between the inner air and the external end cap (R_9):

R_9 presents the convection resistance between the inner air and the end cap and is evaluated as in [17]:

$$R_9 = \frac{1}{A_{ec} h_{ec}}, \tag{27}$$

where A_{ec} is the external area of the end cap (m^2), and h_{ec} is the heat transfer coefficient between the inner air and the end cap (W/ m^2-K) and equals the value of h_{ew}.

The motor consists of the two end caps, and for a more straightforward calculation, these parts are assumed to be circular. Accordingly, A_{ec} is defined as [17]:

$$A_{ec} = 2\pi(ros + t_h)^2, \tag{28}$$

where t_h is the thickness of the motor housing (m).

Convection resistance of the air gap (R_{10}):

The heat transfer in the air gap of the motor is determined by the Taylor number (Ta) as [22]:

$$\mathrm{Ta} = \frac{v_r}{\mu}\sqrt{\frac{l_g^3}{r_{or}}}, \tag{29}$$

where v_r is the peripheral velocity of the rotor (m/s), μ is the dynamic viscosity of air (kg/s-m), r_{or} is the outer radius of the rotor (m), and l_g is the radial thickness of the air gap (m).

Then the Nusselt number and the flow condition in the air gap (laminar, turbulent, and vortex) are assessed based on the value of the Taylor number (Ta) as [22]:

$$\begin{cases} \mathrm{Nu} = 2 & \mathrm{Ta} < 41 \quad \text{laminar mode} \\ \mathrm{Nu} = 0.212\,\mathrm{Ta}^{0.63}\mathrm{Pr}^{0.27} & 41 \le \mathrm{Ta}100 \quad \text{vortex mode} \\ \mathrm{Nu} = 0.386\,\mathrm{Ta}^{0.5}\mathrm{Pr}^{0.27} & \mathrm{Ta} > 100 \ \text{turbulent mode} \end{cases}. \tag{30}$$

However, based on different research on several induction motors in the range of 4 kW to 55kW, the amount of Taylor number is always located in the laminar mode; also, in this study, the amount of Taylor number is located in the laminar mode [17]. In this status, the heat is transferred in the air gap by the conduction mechanism, and R_{10} is calculated as [17]:

$$R_{10} = \frac{ln\left(\frac{r_{is}}{r_{or}}\right)}{2\pi k_{air} L_s}. \tag{31}$$

4. Steady-State Thermal Analysis Method

The matrix inversion theory is applied to estimate the steady-state nodal temperatures of the analytical thermal model as:

$$[\mathrm{T}] = [\mathrm{G}]^{-1}[\mathrm{P}], \tag{32}$$

where [T] is the temperature vector, [P] is the power losses vector matrix containing the losses in each node, and [G] is the thermal conductance matrix. The square [G] is defined as:

$$\mathrm{G} = \begin{bmatrix} \sum_{i=1}^{n}\frac{1}{R_{1,i}} & -\frac{1}{R_{1,2}} & \cdots & -\frac{1}{R_{1,n}} \\ -\frac{1}{R_{2,1}} & \sum_{i=1}^{n}\frac{1}{R_{2,i}} & \cdots & -\frac{1}{R_{2,n}} \\ \vdots & \vdots & \ddots & \vdots \\ -\frac{1}{R_{n,1}} & -\frac{1}{R_{n,1}} & \cdots & \sum_{i=1}^{n}\frac{1}{R_{n,i}} \end{bmatrix}, \tag{33}$$

where the main diagonal element on the main diagonal of the matrix is the sum of the network conductances connected to the node n, and G(i, j) is the thermal conductance connecting the nodes i and j.

5. Experimental Evaluation

To effectively validate and evaluate the performance of the created LP thermal model of SynRM and to gain details about the accuracy of the method in the prediction of temperature distribution across the machine's most important sections, an experimental verification stage was carried out. The experiments conducted for the validation of the model are described in brief hereafter.

5.1. DC Thermal Test

The passive cooling (DC test) implemented for the calibration of the slot conductivity and the interfacial gap, the DC stator test was carried out, and the mentioned parameters were tuned. For this experiment, the machine loss was confined to the stator copper losses. The windings of stator phases were connected in series. As the motor is in a stall condition, the air-cooling rate is zero, and the machine is cooled by the natural cooling method. Consequently, to protect the machine from over-temperature conditions and damage, the current applied to the machine is set to 40% of the rated current. In the steady-state condition, the injected power and the temperature of different components of the machine, e.g., windings, end windings, and the housing of the machine, were measured. RTD sensors (PT 100) were installed inside slots, and the end windings of each phase to measure the temperature of the machine winding and the end-winding. Furthermore, the mean temperature of the housing was evaluated by measuring the temperature of several locations of the machine housing by K-type thermocouples.

Fig. 7 illustrates the temperature comparison obtained by the LPTN and the measurements during the DC test by an injected power of 191.1 W, while the ambient temperature was 21.8℃. The assessed joule losses generated in the slots and end-windings are 92.8W and 98.3W, respectively. Moreover, the uncertainty of the experimental housing temperature as calculated by the K-type thermocouples was ± 2.2 °C and for the end winding and slot measured by RTD sensors is ± 0.85°C.

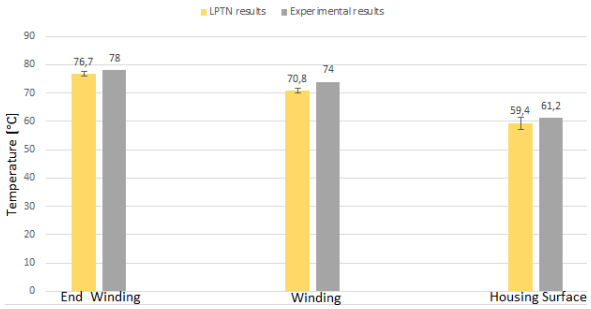

***Fig**. 7. Temperature comparisons during the DC test.*

In the graph, the end winding, the winding, and the housing temperatures are represented. The figure shows good agreement between the predicted and measured temperatures. Further, this test is used for calibration purposes of considering the value of the equivalent thermal conductivity of the slots, length of the interfacial gap, as well as heat transfer resistance between the machine frame and ambient, which is selected correctly. Fig. 8 illustrates the temperature distribution over the housing surface of the motor during the passive cooling.

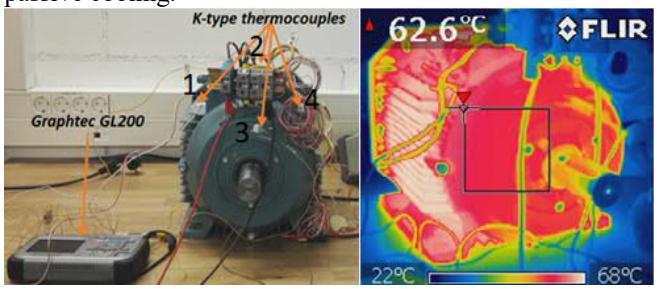

Fig. 8. *Temperature distribution over the housing surface during passive cooling.*

5.2. AC Thermal Test

For the AC test, the SynRM was run in rated speed (1500 r/min). Fig. 9 displays the test bench. During the test, the injected power, the current and voltage, temperature, and power factor of each phase were measured with a data acquisition system (Dewetron). The power losses in the SynRM are composed of resistive losses, iron losses, and mechanical losses. Table 8 shows the value of losses for the AC thermal test (no-load condition) that they were determined experimentally in the rated voltage and frequency. Besides, these values were applied as the losses sources in the LPTN and thermal analysis of the machines. The experimental measurement of losses was presented in our previous research paper [34].

Table 8 Losses of the machine under no-load condition

Name	Symbol	Unite	Value
Stator winding losses	P_{cu}	W	68.50
Iron losses	P_{Fe}	W	125.98
Mechanical losses	P_m	W	33.47

For the thermal experiment, the SynRM was equipped with six RTD sensors. Three RTDs were installed in the end winding part of each phase, and the other three were located inside the slots. The housing temperature of the SynRM was measured by an infrared laser digital thermometer. When the machine reached its steady-state condition, the housing and ambient temperatures and injected power were measured.

Fig. 9. *AC experiment.*

Fig. 10 illustrates the temperature comparison obtained by the analytical thermal model and measurements during the AC test. The relative difference of the analytical results for the housing, slot, and end-winding temperature are 3%, 3.3%, and 6.8%, respectively. These differences in the analytical model arise from the assumption of the uniform distribution of losses in the SynRM as well as the fact that the analytical LP model assesses the mean temperature of the motor parameters while in the experiment, the thermal sensors indicate the temperatures at located points. Fig. 11 indicates the temperature distribution over the housing of the machine in the steady-state condition. The figure provides an overview of the temperature differences in the housing of the SynRM.

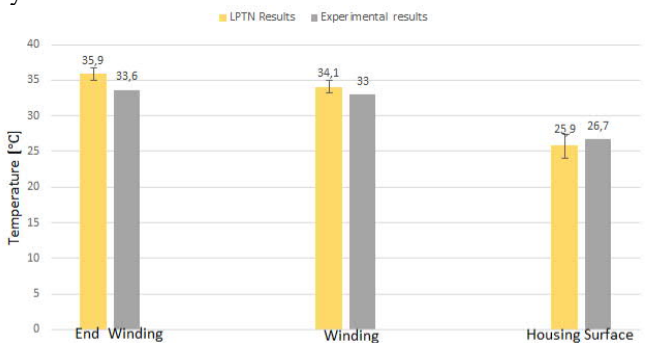

Fig. 10. *Temperature comparisons during the AC test.*

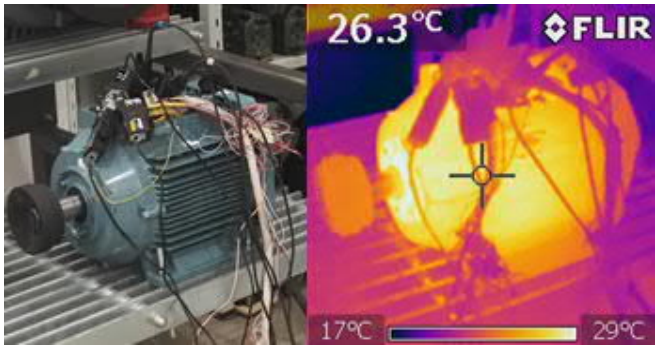

Fig. 11. *Temperature distribution over the SynRM housing.*

6. Conclusion

The principles of the lumped parameter thermal network of the SynRM was presented in this paper. Particular focus was put on to calculate the heat transfer resistance from the machine surfaces during the active and passive cooling. The area-based composite correlations method was proposed to determine the natural and forced convection coefficients from the machine-housing surface and was presented in detail. Furthermore, the simplified method to calculate the radiation coefficient from the complex surface of the TEFC machine is described. Well-proven formulations were employed to calculate the critical parameters of the LPTN.

The experimental results demonstrated that the proposed LP thermal model could forecast the temperature in different parts of the machine with better accuracy (around ±3°C) than what presented in [17] (which accuracy of the model in that research is ±5°C).

7. Acknowledgments

This work has been supported by the European Regional Development Fund within the Activity 1.1.1.2 "Post-doctoral Research Aid" of the Specific Aid Objective 1.1.1 "To increase the research and innovative capacity of scientific institutions of Latvia and the ability to attract external financing, investing in human resources and infrastructure" of the Operational Programme "Growth and Employment" (No.1.1.1.2/VIAA/3/19/501).

8. References

[1] P. Shams Ghahfarokhi, A. Kallaste, A. Belahcen, and T. Vaimann, "Analytical thermal model and flow network analysis suitable for open self-ventilated machines," *IET Electr. Power Appl.*, Feb. 2020.

[2] P. Shams Ghahfarokhi, A. Kallaste, T. Vaimann, and A. Belahcen, "Thermal Analysis of Totally Enclosed Fan Cooled Synchronous Reluctance Motor-state of art - IEEE Conference Publication," in *IECON 2019 - 45th Annual Conference of the IEEE Industrial Electronics Society*, 2019, pp. 1–5.

[3] P. S. Ghahfarokhi, A. Belahcen, A. Kallaste, T. Vaimann, L. Gerokov, and A. Rassolkin, "Thermal analysis of a SynRM using a thermal network and a hybrid model," in *Proceedings - 2018 23rd International Conference on Electrical Machines, ICEM 2018*, 2018, pp. 2682–2688.

[4] K. Grace, S. Galioto, K. Bodla, and A. M. El-Refaie, "Design and Testing of a Carbon-Fiber-Wrapped Synchronous Reluctance Traction Motor," *IEEE Trans. Ind. Appl.*, vol. 54, no. 5, pp. 4207–4217, Sep. 2018.

[5] P. B. Reddy, A. M. El-Refaie, S. Galioto, and J. P. Alexander, "Design of Synchronous Reluctance Motor Utilizing Dual-Phase Material for Traction Applications," *IEEE Trans. Ind. Appl.*, vol. 53, no. 3, pp. 1948–1957, May 2017.

[6] S. M. Taghavi and P. Pillay, "A mechanically robust rotor with transverse laminations for a wide-speed-range synchronous reluctance traction motor," *IEEE Trans. Ind. Appl.*, vol. 51, no. 6, pp. 4404–4414, Nov. 2015.

[7] M. Popescu, J. Goss, D. A. Staton, D. Hawkins, Y. C. Chong, and A. Boglietti, "Electrical Vehicles—Practical Solutions for Power Traction Motor Systems," *IEEE Trans. Ind. Appl.*, vol. 54, no. 3, pp. 2751–2762, May 2018.

[8] A. Boglietti, A. Cavagnino, D. Staton, M. Shanel, M. Mueller, and C. Mejuto, "Evolution and Modern Approaches for Thermal Analysis of Electrical Machines," *IEEE Trans. Ind. Electron.*, vol. 56, no. 3, pp. 871–882, Mar. 2009.

[9] C. Micallef, "End winding cooling in electric machines," 2006.

[10] A. Boglietti, A. Cavagnino, and D. Staton, "Determination of critical parameters in electrical machine thermal models," *IEEE Trans. Ind. Appl.*, vol. 44, no. 4, pp. 1150–1159, 2008.

[11] S. Nategh, H. Zhang, O. Wallmark, A. Boglietti, T. Nassen, and M. Bazant, "Transient Thermal Modeling and Analysis of Railway Traction Motors," *IEEE Trans. Ind. Electron.*, vol. 66, no. 1, pp. 79–89, Jan. 2019.

[12] Y. Gai *et al.*, "Cooling of automotive traction motors: Schemes, examples, and computation methods," *IEEE Trans. Ind. Electron.*, vol. 66, no. 3, pp. 1681–1692, Mar. 2019.

[13] G. Traxler-Samek, R. Zickermann, and A. Schwery, "Cooling airflow, losses, and temperatures in large air-cooled synchronous machines," *IEEE Trans. Ind. Electron.*, vol. 57, no. 1, pp. 172–180, Jan. 2010.

[14] J. A. Malumbres, M. Satrustegui, I. Elosegui, and M. Martínez-Iturralde, "Coupled thermal and hydraulic algebraic models for an open self-ventilated induction machine," *IET Electr. Power Appl.*, vol. 9, no. 8, pp. 513–522, Sep. 2015.

[15] S. Nategh, Z. Huang, A. Krings, O. Wallmark, and M. Leksell, "Thermal Modeling of Directly Cooled Electric Machines Using Lumped Parameter and Limited CFD Analysis," *IEEE Trans. Energy Convers.*, vol. 28, no. 4, pp. 979–990, Dec. 2013.

[16] P. H. Mellor, D. Roberts, and D. R. Turner, "Lumped parameter thermal model for electrical machines of TEFC design," *IEE Proc. B Electr. Power Appl.*, vol. 138, no. 5, p. 205, 1991.

[17] A. Boglietti, A. Cavagnino, M. Lazzari, and M. Pastorelli, "A simplified thermal model for variable-speed self-cooled industrial induction motor," *IEEE Trans. Ind. Appl.*, vol. 39, no. 4, pp. 945–952, Jul. 2003.

[18] J. Lindström, "Thermal Model of a Permanent-Magnet Motor for a Hybrid Electric Vehicle," CHALMERS UNIVERSITY OF TECHNOLOGY, Goteborg, 1999.

[19] A. M. EL-Refaie, N. C. Harris, T. M. Jahns, and K. M. Rahman, "Thermal Analysis of Multibarrier Interior PM Synchronous Machine Using Lumped Parameter Model," *IEEE Trans. Energy Convers.*, vol. 19, no. 2, pp. 303–309, Jun. 2004.

[20] P. Shams Ghahfarokhi, A. Kallaste, A. Belahcen, T. Vaimann, and A. Rassõlkin, "Hybrid thermal model of a synchronous reluctance machine," *Case Stud. Therm. Eng.*, vol. 12, pp. 381–389, Sep. 2018.

[21] F. P. Incropera, D. P. DeWitt, T. L. Bergman, and A. S. Lavine, *Fundamentals of Heat and Mass Transfer*. 2007.

[22] D. Staton, A. Boglietti, and A. Cavagnino, "Solving the More Difficult Aspects of Electric Motor Thermal Analysis in Small and Medium Size Industrial Induction Motors," *IEEE Trans. Energy Convers.*, vol. 20, no. 3, pp. 620–628, Sep. 2005.

[23] A. Boglietti, E. Carpaneto, M. Cossale, S. Vaschetto, M. Popescu, and D. A. Staton, "Stator winding thermal conductivity evaluation: An industrial production assessment," *IEEE Trans. Ind. Appl.*, vol. 52, no. 5, pp. 3893–3900, Sep. 2016.

[24] M. Markovic, L. Saunders, and Y. Perriard, "Determination of the Thermal Convection Coefficient for a Small Electric Motor," in *Conference Record of the 2006 IEEE Industry Applications Conference Forty-First IAS Annual Meeting*, 2006, vol. 1, pp. 58–61.

[25] O. Meksi and A. O. Vargas, "Numerical and experimental determination of external heat transfer coefficient in small TENV electric machines," in *2015 IEEE Energy Conversion Congress and Exposition (ECCE)*, 2015, pp. 2742–2749.

[26] A. Boglietti, A. Cavagnino, M. Parvis, and A. Vallan, "Evaluation of radiation thermal resistances in industrial motors," *IEEE Trans. Ind. Appl.*, vol. 42, no. 3, pp. 688–693, May 2006.

[27] V. D. Rao, S. V. Naidu, B. G. Rao, and K. V. Sharma, "Heat transfer from a horizontal fin array by natural convection and radiation—A conjugate analysis," *Int. J. Heat Mass Transf.*, vol. 49, no. 19, pp. 3379–3391, 2006.

[28] M. Ahmadi, G. Mostafavi, and M. Bahrami, "Natural convection from rectangular interrupted fins," *Int. J. Therm. Sci.*, vol. 82, pp. 62–71, 2014.

[29] "Motor-CAD Software by Motor Design - EMag, Therm and Lab." [Online]. Available: https://www.motor-design.com/motor-cad-software/.

[30] P. Shams Ghahfarokhi, A. Kallaste, T. Vaimann, and A. Belahcen, "Natural convection from flat side's of coil system," in *2018 19th International Scientific Conference on Electric Power Engineering (EPE)*, 2018, pp. 1–5.

[31] P. Shams Ghahfarokhi, "Development of Thermal Analysis Tools for Synchronous Reluctance Motors - TalTech raamatukogu digikogu," Tallinn University of Technology, 2019.

[32] D. A. Staton and A. Cavagnino, "Convection Heat Transfer and Flow Calculations Suitable for Electric Machines Thermal Models," *IEEE Trans. Ind. Electron.*, vol. 55, no. 10, pp. 3509–3516, Oct. 2008.

[33] A. Boglietti and A. Cavagnino, "Analysis of the endwinding cooling effects in TEFC induction motors," *IEEE Trans. Ind. Appl.*, vol. 43, no. 5, pp. 1214–1222, 2007.

[34] P. Shams Ghahfarokhi, A. Kallaste, T. Vaimann, and A. Belahcen, "Power Losses Analysis in Thermal Design of a Synchronous Reluctance Motor," in *2019 IEEE 60th International Scientific Conference on Power and Electrical Engineering of Riga Technical University (RTUCON)*, 2019, pp. 1–5.